Effects of alkali cations and halide anions on the DOPC lipid membrane

Robert Vácha[1], Shirley W. I. Siu[2], Michal Petrov[1], Rainer A. Böckmann[2], Justyna Barucha-Kraszewska,[3] Piotr Jurkiewicz,[3] Martin Hof,[3] Max L. Berkowitz[4*] and Pavel Jungwirth[1*]

[1]*Institute of Organic Chemistry and Biochemistry, Academy of Sciences of the Czech Republic and Center for Biomolecules and Complex Molecular Systems, Flemingovo nám. 2, 16610 Prague 6, Czech Republic*

[2]*Theoretical & Computational Membrane Biology, Center for Bioinformatics, Saarland University, P.O. Box 15 11 50, 66041 Saarbrücken, Germany*

[3]*J. Heyrovsky Institute of Physical Chemistry, Academy of Sciences of the Czech Republic, v. v. i., Dolejskova 3, 18223 Prague 8, Czech Republic*

[4]*Department of Chemistry, University of North Carolina,Chapel Hill, North Carolina, 27599*

**Corresponding authors: pavel.jungwirth@uochb.cas.cz (P.J.) and maxb@unc.edu (M.L.B.)*

Abstract

By means of molecular dynamics simulations with an all-atom force field we investigated the affinities of alkali cations and halide anions for the dioleoylphosphatidylcholine lipid membrane in aqueous salt solutions. In addition, changes in phospholipid lateral diffusion and in headgroup mobility upon adding NaCl were observed using fluorescence spectroscopy. The simulations revealed that sodium is attracted to the headgroup region with its concentration being maximal in the vicinity of the phosphate groups. Potassium and cesium, however, do not preferentially adsorb to the membrane.

Similarly, halide anions do not exhibit a strong affinity for the lipid headgroups but merely compensate the positive charge of the sodium counter-cations. Nevertheless, larger halides such as bromide and iodide penetrate deeper into the headgroup region toward the boundary with the hydrophobic alkyl chain; this effect being likely underestimated within the present non-polarizable force field. Addition of alkali halide salts modifies physical properties of the bilayer including the electronic density profiles, the electrostatic potential, and the area per lipid headgroup.

Introduction

Electrolyte solutions strongly influence physico-chemical properties of model lipid membranes. To explain this influence, much of the theoretical work often relies on classical Gouy-Chapman mean-field type theory that predicts the same type behavior for ions of the same valency[1]. The importance of the specific ionic effect for membrane biophysics was noticed by Hodgkin and Horowicz who observed that different anions produce different effects on the muscle twitch tension.[2] The increase of the ionic effect followed the series Cl^- <Br^-< I^-<SCN^-. Hodgkin and Horowicz observed that ordering of the anions in the above series is correlated to their lyotropic character and therefore they proposed that it is related to the degree of adsorption of anions to the muscle membranes. Later measurement of the membrane dipole potential [3] showed that dipole potentials are reduced in the presence of salts and the anion effectiveness follows the series ClO_4^->SCN^->I^->Br^->Cl^->F^->SO_4^{2-}. It was assumed that the reduction in the dipole potential correlates with the degree of ion adsorption to the membrane. It was also noticed that the ordering of the anions coincides with the reverse Hofmeister series [4]. More recently, the results from the osmotic stress measurements [5-7] of the interaction between lamellar membranes in different aqueous salt solutions were also interpreted as confirming the conclusion obtained from the dipole potential measurements, i.e., that the specific ionic effect follows the reverse Hofmeister series. The interpretation of the results from the osmotic stress experiments is somewhat involved and very recent experiments, which studied nanomechanics of lipid bilayers by force spectroscopy [8] and ion binding to solid supported lipid membranes, [9] provide a more direct information on the location of ions next to lipid membranes. While the former showed an increase in lateral phospholipid-phospholipid interactions upon addition of salt [8], results from experiments on solid supported membranes indicated that weakly hydrated anions and strongly hydrated

cations are attracted to the membrane [9]. It has been also shown by combination of various experimental techniques that cations significantly influence neutral lipid bilayers [10,11].

Detailed information about location of ions with respect to lipid membranes can also be obtained from molecular dynamics simulations; indeed, first simulations that studied ionic aqueous solutions next to neutral zwitterionic membranes pointed out that cations and anions create a double layer at the membrane/water interface.[11,12] Specifically, it was observed that at the interface between aqueous solutions and membranes containing phosphatidylcholine (PC) headgroups, Na^+ penetrates into the headgroup region while Cl^- does not. Further simulations confirmed these observations, although detailed locations of the ions were somewhat depending on the force fields used in the simulations.[13-15] Simulations also investigated location of different cations, i.e., monovalent, divalent [16] or even trivalent[17] ions next to membranes, while using the same counter-anion (Cl^-).

Understanding of the intricate details about the location of ions at the aqueous solution/membrane interface is very important for our understanding of the mechanisms of membrane-membrane and membrane-peptide interactions that are modulated by the values of surface potentials. The location of the ions at the aqueous solution/membrane interface also sets up the value and character of the transmembrane potential, which in turn regulates the traffic across membranes. In the present paper we report on computational and experimental work we performed to study the influence of salt on a bilayer containing dioleoylphosphatidylcholine (DOPC) phospholipid molecules. Using molecular dynamics simulations technique we systematically studied the effect of different ions, i.e., alkali cations and halide anions, on the properties of the DOPC/aqueous solution interface. In our study we first considered monovalent salts containing a common Cl^- anion with different cations such as Na^+, K^+, and Cs^+. Next, we considered salts containing a common cation (Na^+) but different anions, such as Cl^-, Br^- and I^-. If we consider Na^+ and Cl^- as our reference ions, we

can infer from our simulations how the change of the character of the ions, varying from more strongly hydrated to less strongly hydrated compared to the reference ions, influences the lipid membrane/ ionic solution interface. In this respect our simulations can be compared directly with the results from the recent experiments on solid supported membranes [9]. Additionally, we employed fluorescence spectroscopy to study how the presence of NaCl salt influences the properies of DOPC bilayers.

Methods

Computational

All molecular dynamics simulations were performed using the GROMACS program package [18]. We simulated five different systems, each containing 72 DOPC lipid molecules, 2627 water molecules, and 100 ions (i.e., 50 cations and 50 anions). Each system contained a specific salt - NaCl, KCl, CsCl, NaBr, or NaI. The employed numbers of water molecules and ions yield a formal 1 M concentration of salt. This higher than the physiological concentration was used since Hofmeister effects are typically studied at molar ionic strengths. Moreover, higher concentrations of ions help to improve sampling.

The initial configuration of the system was taken from our previous study [19] where we equilibrated a DOPC membrane for 100 ns in pure water. Ions were inserted in the water phase and, after energy minimization and 80 ns of equilibration, 120 ns production runs were carried out with a 2 fs time-step. The system was kept within $NP\gamma T$ ensemble with surface tension of 22 dyn/cm in the membrane plane and pressure of 1 atm in perpendicular direction and 310 K using Berendsen barostat and thermostat. Barostat scaling time was 1 ps with compressibility of 4.5 10^{-5} bar^{-1}, while the thermostat time constant was set to 0.1 ps. The van der Waals and Coulomb interactions were cut-off at 1.2 nm and the long-range Coulomb

interactions were accounted for using the Particle Mesh Ewald (PME) Method [20]. Lipids were described by a recently developed all-atom forcefield based on the Generalized Amber Force Field [19]. For water we employed the SPC/E model[21] and parameters for ions are presented in Table 1. The reason for using this parameterization for ions[22-25] is twofold. While it was originally developed with a polarizable water model, it is also consistent with the presently employed SPC/E water, as demonstrated recently[26]. Moreover, the standard AMBER ion parameterization leads to an artificially strong ion pairing (particularly for potassium) [26,27], therefore, we were avoiding it.

In order to quantify the properties of DOPC bilayer/aqueous interface we evaluated density profiles of individual species and electrostatic potentials along the normal to the bilayer. We also calculated the average number of adsorbed ions per lipid and the corresponding mean adsorption times. The former was defined as the number of ions within the distance of 0.6 nm from a phosphorus atom of any phosphate group divided by the number of lipid molecules. The choice of the phosphate center is particularly suitable for the cations. The radius of 0.6 nm was chosen to be large enough to create a continuous volume from overlaping spheres on neighboring lipid headgroups and to account also for the ion adsorption in the carbonyl region. For anions we additionally counted the number of ions within 0.6 nm from the nitrogen of choline as a center of positive charge on lipids.

Experimental

Fluorescence solvent relaxation (SR) and fluorescence correlation spectroscopy (FCS) measurements were performed on DOPC (Avanti Polar Lipids, Alabaster, AL) bilayer. The chloroform lipid solution was mixed with appropriate fluorescent dye. 6-dodecanoyl-2-dimethylaminonaphthalene (Laurdan) (Invitrogen) or 4-[(*n*-dodecylthio)methyl]-7-(*N*,*N*-dimethylamino)-coumarin (DTMAC) (synthesized and purified as described in [28]) were used

for SR measurements in 1:100 dye/lipid molar ratio. 2-(4,4-difluoro-5,7-dimethyl-4-bora-3a, 4a-diaza-s-indacene-3-dodecanoyl) -1-hexadecanoyl-sn-glycero-3- phosphocholine (Bodipy C12-HPC) (Invitrogen) was used for FCS in 1:100 000 dye/lipid molar ratio. The organic solvents were evaporated and the lipid film was suspended in water (Milli-Q3 system, Millipore, Etten-Leur) or 150mM NaCl solution. The obtained multilamellar vesicles were either extruded through polycarbonate membranes (Avestin, Ottawa, Canada) with 100 nm pores (SR) or sonicated (FCS).

Supported phospholipid bilayers (SPBs) were formed directly in the measurement cell by exposing freshly cleaved mica (Metafix, Montdidier, France) to 0.2 mM (lipid concentration) suspension of sonicated vesicles in 150 mM NaCl as described in [29]. The suspension was stirred continuously during 4 hours of incubation. Unbound vesicles were removed by flushing with 50 mL of 150 mM NaCl. For the FCS measurements in pure water, the NaCl solution was replaced after SPB creation with pure water by slow flushing. The experiments were performed at (10 ± 0.5)°C (SR) and at (23 ± 2)°C (FCS).

SR is a unique tool for measuring hydration and mobility of fully hydrated free standing phospholipid membranes [30]. Fluorescence spectra and decays were recorded on a Fluorolog 3 (Jobin Yvon) and on an IBH 5000 U SPC equipped with an IBH laser diode NanoLED 11 and a cooled Hamamatsu R3809U-50 microchannel plate photomultiplier, respectively. The time-resolved emission spectra (TRES) were gained by the spectral reconstruction method [31] from a set of emission decays recorded at a series of wavelengths spanning the steady-state emission spectrum. The total emission shift $\Delta\nu$ and the mean integrated relaxation time τ_r, which reflect bilayer hydration and mobility, respectively, were calculated as previously described [31].

FCS experiments were carried out on a MicroTime 200 inverted confocal microscope (Picoquant, Germany). The configuration contained a pulsed diode laser (LDH-P-C-470, 470

nm, Picoquant, Germany), a proper filter set (clean up filter HQ470/20, dichroic mirror 490DRLP, and band-pass filter HQ525/50) (Omega Optical), and a water immersion objective (1.2 NA, 60×) (Olympus). Measurements of lipid lateral diffusion were performed by the *Z*-scan method [32], which was shown to be the only artifact-free single focus measurement of lateral diffusion coefficients [33]. A set of FCS curves was measured at various *Z* positions of the focal plane with respect to the bilayer spaced by 0.2 μm. Particular FCS curves were treated according to [32] and the obtained diffusion times were plotted versus normalized particle number as described in [34,35] to obtain the effective diffusion coefficient D_{eff} and the intercept with diffusion time axis characterising the type of diffusion (i.e. free or hindered) [34,35]. Fluorescence intensity scans were recorded at the plane of the bilayer and at a plane perpendicular to it to check for bilayer confluence.

Results

Computational

A representative snapshot from a MD simulation of the DOPC bilayer in the NaI solution is depicted in Figure 1. For sake of clarity and easy comparison we present the results by first looking at salts of different cations with the same Cl^- counter-anion and then at salts with different anions in the presence of the common Na^+ counter-cation.

CATIONS

Ion adsorption

Total and partial electron density profiles for systems containing Cl^- anion and different counter-cation are shown in Figure 2. Note that the total electron density profiles are very similar, nevertheless there are substantial differences in partial density profiles of ions. Two issues are of particular concern when discussing ion adsorption to the lipid bilayer - the

amount of adsorbed ions and their preferred location. These were analyzed further by calculating the number density profiles that are shown in Figure 3. From this figure we can see that sodium ions are preferentially enhanced in the phosphate region. This is followed by a weaker adsorption of chloride at the outer part of the membrane (i.e., within the choline region). Larger sized cations such as cesium only weakly penetrate into the headgroup region and do not display a density peak, similar to the behavior of their counterions (chloride). Potassium is located somewhere between sodium and cesium, penetrating the membrane but not having a significant enhancement there. In Figure 3 we can also see that peaks of choline groups are in different locations depending on the identity of the cation, which indicates a change in the headgroup tilt in different salts.

To define the number of the adsorbed ions to the membrane we used the adsorption criteria described in the Methods section. We present the number of adsorbed ions in Table 2. There are about 0.3 sodium cations per lipid molecule in the phosphate region, while there are only 0.2 potassium and 0.1 cesium ions. This means that there is one sodium per every three lipids but merely one cesium for ten lipids in the membrane. While the absolute numbers depend somewhat on the definition of the adsorption volume, the ratio between different adsorbed cations is robust. Note, that when we use for the adsorbed anions the definition of the volume around choline groups, the number of adsorbed chlorides is reaching the same value as the number of adsorbed sodium cations (compensating its charge). For the case of CsCl, using this definition the total number of adsorbed Cl^- overrides the number of adsorbed Cs^+.

Additional important parameters describing binding of ions to the membrane surfaces are the average residence time and the duration of the longest contact, which were calculated as the mean and the longest time that cations spend without interruption within the distance of 0.6 nm from phosphate atoms. The calculated values are given in Table 3. The order of

magnitude difference in residence times of individual cations is in agreement with the notion of deeper penetration and stronger adsorption at the membrane surface by sodium ions compared to potassium and cesium.

Electrostatics

The electrostatic potentials were calculated by solving the Poisson equation using the periodic boundary conditions as in Reference [36]. The absolute value was set to zero in the center of the solution (Figure 4). The total electrostatic profiles are similar to each other for all electrolytes as shown in Figure 4A. The residual differences occur at the headgroup region where the adsorption of ions causes a small change of the electrostatic potential compared to the system without salts. A larger increase in the surface potential compared to the case of pure water is observed for NaCl than for KCl. Moreover, the electrostatic potential in the headgroup region displays a significant decrease for the case of CsCl solution when compared to the situation in pure water. Note that the potential remains practically equal to zero in the aqueous phase until it sharply rises at the edge of the membrane. The zero value close to the edge of the membrane means that the zeta potential for these systems also vanishes.

Unlike the total profiles, the partial electrostatic profiles of water, ions, and lipids differ dramatically for the studied systems (Figure 4B). The differences in profiles due to lipids are caused by change of the orientation of lipid headgroup dipoles. Electrostatic potential of ions clearly show that adsorption of NaCl at the membrane surface creates a dipolar layer (with opposite orientation to the lipid dipoles). Due to lack of appreciable adsorption, CsCl does not have a large contribution to the electrostatic profile. The effect of KCl is somewhat between NaCl and CsCl. However, the orientation of water molecules at the headgroup region compensates almost perfectly the effect of salts. This compensation leads to the above observation that the total electrostatic profiles are very similar to each other.

Area per lipid & membrane thickness

We investigated how the area per lipid changes depend on the type of cation present in the system. It was calculated as the lateral area of the simulation box in the membrane plane divided by the number of lipids in a single layer. For a given size of unit cell we observed relatively large fluctuations in these areas, up to 0.1nm^2 per lipid for the time scale over 100 ns. The average areas per lipid are given in Table 4. It can be seen that, compared to neat water, the area per headgroup decreases by around 5% in the presence of salts with the Cl^- anion and different alkali cations, which is the same trend as observed in previous simulations of POPC lipid bilayers [11]. The observed decrease of area per lipid correlates with an increase of the membrane thickness. Note that the membrane thickness was measured as in the experiment [37], i.e. as the distance between the two peaks in the electron density profiles of the system (Table 2.). As for the area per lipid, the specific effect of different alkali cations is small.

ANIONS

Ion adsorption

As shown in Figure 5, the electron density profiles are very similar for all salts with varying anions. At the same time differences in anion adsorption can be clearly seen from the number density plots on Figure 6. This figure shows that larger anions, such as I^-, penetrate deeper into the membrane compared to small anions such as Cl^- . From the number density profiles it also follows that sodium adsorb slightly stronger in the presence of larger counter-anions, however the differences in counter-ion adsorption are very small and within the statistical error. The penetration of iodide into the headgroup region is graphically

demonstrated in Figures 7-8 which provide an overall and a zoomed in view on the local environment around this anion at membrane.

The number of adsorbed ions at the membrane is shown in Table 2. There is roughly the same number of the anions within 0.6 nm from the phosphates, while the volume around choline group contains more larger-sized anions (such as I^-) than smaller ones (Cl^-). A similar result was obtained when the number of ions within 0.6 nm from any lipid atom was analyzed. As already mentioned above, there are about 0.3-0.4 sodium cations per lipid in the phosphate region (see Table 2), with the number of Na^+ in membrane slightly increasing with the size of the counter-anion. Table 5 shows the residence times of sodium, depending on the type of anion, which are increasing from chloride to iodide. Interestingly, the longest time for which the Na^+ ion stayed adsorbed somewhat decreases as the size of counter-ion increases.

Electrostatics and headgroup orientation

For the investigated salts there is virtually no anion-specific effect of electrostatic potential across the membrane, as can be seen from Figure 9. Unlike the case of varying cations, the partial electrostatic profiles for different anions are also very similar to each other (data not shown here). As for the varying cations, we see that for varying anions the potential remains zero close to the membrane. It is worth mentioning that there is a significant difference in the distributions of headgroup orientation in different solutions, as can be seen from Table 6. This orientation was computed as the angle between the vector connecting the phosphorus and the nitrogen atoms and the normal to the bilayer. Even though the distribution is quite broad it is clear that ion adsorption leads to the orientation of headgroups more outwards the membrane (heads stand more “straight”), this effect being stronger for larger anions. Note, that larger cations (Cs^+) which are not enhanced at the head group region have

an opposite effect, with the heads being oriented more in the membrane plane (heads "lay down").

Area per lipid

The effects of the anions on the area per lipid were analyzed in the same way as for the cations. The mean values of areas per lipid and related membrane thickness values, which are not strongly anion-dependent, are presented in Table 4. As in the case of cations we also observed large fluctuations in the membrane area, up to 0.1 nm^2/per lipid over 100 ns time period. To be confident that we reached equilibrium, simulations for NaBr were extended up to 300 ns and we have not observed any transition or shift in the mean area per lipid during this time period.

Experimental

The effect of NaCl on the DOPC model membrane was studied experimentally using fluorescent time-resolved solvent relaxation technique and z-scan fluorescence correlation spectroscopy, allowing determination of headgroup hydration and mobility, and lateral diffusion, respectively. For both methods two identical bilayer systems with or without 150 mM NaCl were compared. Since already a 150 mM concentration was found to produce measurable changes, it was chosen as the physiologically relevant one. This choice also minimizes artifacts which could arise in FCS measurements if the refractive index of the sample differs appreciably from that of pure water.

SOLVENT RELAXATION

SR experiments were performed using two fluorescent probes, Laurdan and DTMAC, which were shown to be located at two different depths of the bilayer, i.e. at the level of *sn*-1

carbonyl and at upper glycerol region [38,39]. The parameters obtained from the TRES analysis, i.e. the total emission shift ($\Delta\nu$), the mean integrated relaxation time (τ_r), and the percentage the relaxation process, which was observed, are listed in Table 7.

Analysis of the full-width at half-maximum of TRES revealed that more than 70% of the relaxation process was captured within the experimental time window (0.05–30 ns), which means that the time-dependent Stokes shift is mainly occurring on the nanosecond time scale. No polarity changes of the local environment of the dyes with salt were observed, as seen from the constant $\Delta\nu$ values. This parameter is usually attributed to the extent of membrane hydration since water is the main source of polarity in lipid membranes. However, the relaxation kinetics for Laurdan was slowed down by about 7 % upon the addition of NaCl, as revealed by the τ_r values. The difference is not large but it is significant (i.e., above the resolution of the measurement). A vanishing salt effect is observed for the DTMAC probe located closer to the bulk water, i.e. at the upper glycerol level. It should be pointed out, that we showed earlier that DTMAC is less sensitive than Laurdan to changes in the headgroup region [38,39]. These results indicate that the mobility of hydrated lipid headgroups is somewhat more restricted in the presence of NaCl when compared to the pure water.

Z-SCAN FCS

The obtained intensity scans show confluent DOPC SPBs in both pure water and NaCl solution. No intensity loss was observed upon medium exchange. Since no buffer and no calcium was present during SPB formation, some fraction of vesicles adhered to the bilayer are present even after flushing [29]. This was observed as short initial decrease of the fluorescent signal due to photobleaching of these immobile vesicles. Thanks to this fast bleaching no fluorescent signal from the adhered vesicles was collected during the Z-scan.

The results obtained for DOPC SPBs in NaCl and in pure water are presented in Table 8. The lateral diffusion in the NaCl solution is considerably (by more than 25 %) slower than in pure water. The intercept of the diffusion time as a function of particle number with diffusion time axis is close to 0, which means that predominantly free diffusion is observed (see [34,35] for detailed explanation). All the values shown in the table are averages for at least two samples, every sample z-scanned at two different spots before and after medium exchange. The above results show that the lateral diffusion of lipids in DOPC supported bilayer is somewhat restricted in the NaCl solution when compared to water.

Discussion

First, let us consider the effect of the presence of different cations, such as Na^+, K^+ or Cs^+ (with the Cl^- counter-ion) in the system. We observe in the simulations that sodium ions adsorb to the DOPC membrane, being preferentially located at the phosphate region. This also enables co-adsorption of chloride at the choline region, which is located in the outer part of the membrane. The Na^+ and Cl^- ions thus create an electric double layer, which is almost fully compensated by the orientation of waters, so that the total electrostatic profile is similar to the system without salt. In contrast, larger cations, such as cesium, do not preferentially adsorb to the membrane and only weakly penetrate the headgroup region. Potassium exhibits an intermediate behavior between sodium and cesium, penetrating the membrane, but not being enhanced in the membrane region. Moreover, neither of the CsCl and KCl salts creates an ionic double layer at the membrane surface.

Our findings qualitatively agree with the results from previous simulations that smaller cations adsorb more to the membrane than larger cations [13-15]. However, our study shows a quantitative difference in the exact location where sodium ions display a peak in the density profile. Employing an all-atom forcefield, we find that sodium is primarily enhanced at the

phosphate region, while in the previous studies which used a united atom force field, sodium preferred the carbonyl region or that between the carbonyls and phosphate [11-15,40,41]. Also, potassium behavior at the membrane seems to be somewhat forcefield dependent - within the present simulations K^+ was not enhanced in the membrane as is the simulations with OPLS potassium [14,15], while that described using the CHARMM forcefield exhibits a stronger attraction for the headgroup region [13].

Next, we consider the effect of having different halide anions paired with a common sodium counter-cation. We observe a stronger affinity of anions for the membrane as we move from Cl^- to Br^- and to I^-. In other words, larger anions penetrate deeper into the membrane than smaller ones, similar to the finding in a previous computational study of a POPC membrane[42,43]. Nevertheless, we find that the differences in anion behavior are small and none of the halides is actually enhanced at the membrane, although iodide penetrates deeper into the membrane. That we observe only a small difference in anion behavior at the membrane/aqueous solution interface may, however, be due to deficiencies of the non-polarizable force fields. It was demonstrated in the simulations of ions in water clusters [44] and ions at the water-air interface [45] that inclusion of polarization enhances the surface affinity of soft ions such as the heavier halides. Such simulations for membranes are unfortunately computationally extremely demanding, moreover a reliable polarizable potential is not available for these systems. We are currently developing and testing a polarizable force field for phospholipid membranes, which will allow for directly addressing this issue and connecting more quantitatively to the experiment[8,9].

Both fluorescence experiments performed in this study show trends upon adding salt which are consistent with the computational prediction of affinity and direct interaction of sodium with the bilayer. Measurements show that the presence of sodium ions rigidifies the headgroup region. Also, interaction of sodium cations with hydrated oxygen atoms in the

headgroup slows down the lateral and rotational diffusion of the DOPC headgroup within the bilayer. The two employed experimental approaches are based on very different concepts (i.e., while solvent relaxation is based on monitoring photophysics occurring on the nanosecond timescale, FCS analyses fluorescence fluctuations on the millisecond timescale). Nevertheless, the effect of added salt on the behavior of the aqueous bilayer (with the fluorescence label) is consistently revealed as in a similar study of POPC [11].

It should be stressed that MD simulations, such as those presented here, are necessarily limited in their dimensional and temporal scope and can, therefore, only partially relate to the present experiments. For example, large scale fluctuations within the membrane can possibly lead to creation of pores, through which water and even ions could penetrate. Such effects, which can be present in many experiments, could not be addressed by the present simulations. It is also worth stressing that different experimental probes and techniques cannot be expected to be influenced to the same extent by salts since some membrane properties, such as headgroup orientation and diffusion, are more sensitive to specific ion effects than others, such as, for example, membrane thickness.

In summary, there are several physical mechanisms which determine ion-specific adsorption to aqueous DOPC membrane. Ion pairing drives small alkali cations to the negatively charged phosphate and carbonyl groups of the phospholipids. Anions are analogously, albeit more weakly attracted to the positively charged choline groups. In addition, large and soft ions can penetrate and even be enhanced at the boundary between the hydrophilic and hydrophobic regions of the membrane. Charge neutralization is another effect to consider. If one type of ions exhibits affinity to the membrane then the counter-ions will also be attracted to ensure interfacial neutrality. Finally, steric hindrance at the crowded headgroup region may prevent ion adsoption or at least create a kinetic barrier. This effect is likely to be particularly important for more compact phases of the bilayer.

Conclusion

Molecular dynamics simulations with an all-atom force field were performed to investigate interactions of alkali cations and halide anions with a DOPC bilayer in aqueous salt solutions. Among the investigated cations, only sodium exibits an enhancement at the headgroup region, its concentration peaking in the vicinity of the phosphate groups. In contrast, potassium or cesium do not adsorb preferentially at the membrane. For anions the situation is different. On one hand, they tend to compensate the positive charge of the sodium counter-cations by weakly accumulating at the outer headgroup region next to the choline groups. On the other hand, larger anions tend to penetrate closer to the hydrophobic region of the membrane due to a mechanism similar to their segregation at the water/vapor interface. This effect is likely to be further enhanced when polarization interactions are included into the force field.

Changes upon adding NaCl were also observed by means of fluorescence spectroscopy for phospholipid lateral diffusion and in solvent relaxation. Compared to neat water, the phospholipid lateral diffusion in 150 mM NaCl is slowed down by about 25 %. Additionally, solvent relaxation in the headgroups is slowed down by ~8 %.

Specific ion effects at the phospholipid membrane influence to varying degrees physical properties of the bilayer. Compared to neat water, changes are observed in the electron density profiles and in the surface potential, as well as in the areas per lipid headgroup. While addition of alkali halide salts leads to non-negligible effects, ion specificity is weak for these properties. This can be contrasted with strongly ion specific density profiles, which indicates that different probing techniques exhibit varying sensitivity to ion specificity.

Acknowledgment

Support from the Czech Ministry of Education (grant LC512) and the Czech Science Foundation (grant 203/08/0114) is gratefully acknowledged. MLB acknowledges support from the National Science Foundation grant MCB-0615469. RAB and SWIS acknowledge support from the Deutsche Forschungsgemeinschaft (Graduate School Structure Formation and Transport in Complex Systems 1276/1). R.V. acknowledges support from the Czech Science Foundation (grant 203/05/H001) and from the International Max-Planck Research School. Part of the work in Prague was supported via Project Z40550506.

Table captions:

Table 1. Force field parameters employed for alkali caltions and halide anions.

Table 2. Mean values and standard deviations of number of ions adsorbed per lipid within a distance of 0.6 nm from phosphates or cholines.

Table 3. Residence times of alkali cations and longest contact times within a distance of 0.6 nm from phosphates. In all cases chloride is the counterion.

Table 4. Average areas per lipid and membrane thickness in different solutions.

Table 5. Residence times and longest contact times of sodium within a distance of 0.6 nm around phosphates for aqueous solutions with different halide counter-anions.

Table 6. Peak maximum and half-width at half-maximum of lipid headgroup orientational distributions. Note that the orientational distributions are asymmetric, therefore, we present two half-widths (left/right from the peak maximum).

Table 7. Solvent relaxation parameters measured for 150 mM NaCl or water suspension of DOPC large unilamellar vesicles labeled with 1 mol% of Laurdan or DTMAC.

Table 8. Effective lateral diffusion coefficient measured in supported DOPC membrane on mica in 150 mM NaCl or in water using FCS Z-scan technique.

Table 1:

	Charge [e]	σ[nm]	ε[kJ/mol]
Na^{+23}	1.000	0.235019	0.54392
K^{+24}	1.000	0.3048655	0.41840
Cs^{+25}	1.000	0.383086	0.41840
Cl^{-22}	-1.000	0.43200	0.41840
Br^{-22}	-1.000	0.47004	0.41840
I^{-22}	-1.000	0.51494	0.41840

Table 2:

	Phosphate volume	Choline volume
NaCl Na^+	0.32 ± 0.03	
NaCl Cl^-	0.09 ± 0.03	0.27 ± 0.04
KCl K^+	0.16 ± 0.03	
KCl Cl^-	0.06 ± 0.03	0.19 ± 0.04
CsCl Cs^+	0.08 ± 0.03	
CsCl Cl^-	0.04 ± 0.02	0.15 ± 0.04
NaBr Na^+	0.34 ± 0.04	
NaBr Br^-	0.09 ± 0.03	0.31 ± 0.04
NaI Na^+	0.38 ± 0.04	
NaI I^-	0.09 ± 0.03	0.34 ± 0.04

Table 3:

	Mean residence time	Time of the longest contact
Na^+	350 ps	120 ns
K^+	83 ps	30 ns
Cs^+	44 ps	3 ns

Table 4:

	Averaged area per lipid [nm^2]	Membrane thickness [nm]
Water[19]	0.72	3.6
NaCl	0.69	3.7
KCl	0.69	3.7
CsCl	0.70	3.7
NaBr	0.69	3.7
NaI	0.70	3.8

Table 5:

	Mean residence times of Na^+	Longest contact time of adsorbed Na^+
NaCl	350 ps	120 ns
NaBr	400 ps	110 ns
NaI	530 ps	90 ns

Table 6:

	Most probable orientation [°]	Half width at half maximum [°]
Water[19]	67	36/37
NaCl	61	38/61
KCl	65	40/45
CsCl	72	34/48
NaBr	57	40/57
NaI	53	43/53

Table 7:

	Laurdan			DTMAC		
	$\Delta\nu$ (cm^{-1})[a]	τ_r (ns)[b]	Observed[c]	$\Delta\nu$ (cm^{-1})[a]	τ_r (ns)[b]	Observed[c]
water	4250 ± 50	1.45 ± 0.05	76%	2350 ± 50	1.12 ± 0.05	71%
NaCl	4250 ± 50	1.56 ± 0.05	77%	2350 ± 50	1.09 ± 0.05	74%

[a] $\Delta\nu = \nu(t=0) - \nu(t=\infty)$; $\nu(t=0)$ – estimated [30], $\nu(t=\infty)$ obtained from TRES reconstruction [31].

[b] Integrated relaxation time: $\tau_r = \int_0^\infty C(t)dt$.

[c] Percentage of observed SR process obtained by comparison of the Δν values calculated using the estimated ν(t=0) with those obtained exclusively from TRES reconstruction [30].

Table 8:

	τ_D (ms)[a]	D_{eff} ($\cdot 10^{-12}$ m^2/s)[b]	intercept (ms)[c]
water	1.74 ± 0.31	7.9 ± 1.3	0.4 ± 0.5
NaCl	2.19 ± 0.12	6.0 ± 0.4	0.18 ± 0.14

[a] Mean diffusion time.
[b] Effective diffusion coefficient.
[c] Intercept of the linear fit to the data with diffusion time axis (i.e. relative particle number = 0).
All the parameters obtained from the plot of apparent diffusion times versus the relative particle numbers as described in [34].

Figure captions:

Figure 1. A representative snapshot of the DOPC bilayer in an aqueous salt solution.

Figure 2. Total and partial electron density profiles. Full lines are for NaCl, dashed lines for KCl, and dashed-dotted lines for CsCl. Only half of the unit cell is depicted with the results being averaged over the two equivalent halves.

Figure 3. Number density profiles of ions at the membrane/solution interface averaged over a 40 ns trajectory segment after equilibration. Full line - NaCl, dashed line – KCl, and dashed-dotted line –CsCl. Choline and phosphate densities are also depicted.

Figure 4. (A) Total and (B) partial electrostatic potentials at the membrane/solution interface for systems with varying cations. Due to symmetry only half of the unit cell is shown.

Figure 5. Total and partial electron density profiles. Full lines are for NaCl, dashed lines for NaBr, and dashed-dotted lines for NaI. Only half of the unit cell is depicted with the results being averaged over the two equivalent halves.

Figure 6. Number density profiles of ions at the membrane/solution interface averaged over a 40 ns trajectory segment after equilibration. Full line - NaCl, dashed line – NaBr, and dashed-dotted line –NaI. Choline and phosphate densities are also depicted.

Figure 7: Top view of the NaI solution/membrane interface. Note that sodium cations (blue) and, in particular, iodide anions (pink) are able to penetrate into the headgroup region.

Figure 8: A detailed snapshot showing the local arrangement of phospholipids around an iodide anion which penetrated deep into the headgroup region..

Figure 9. Total electrostatic potential at the membrane/solution interface for systems with varying anions.

Figure 1:

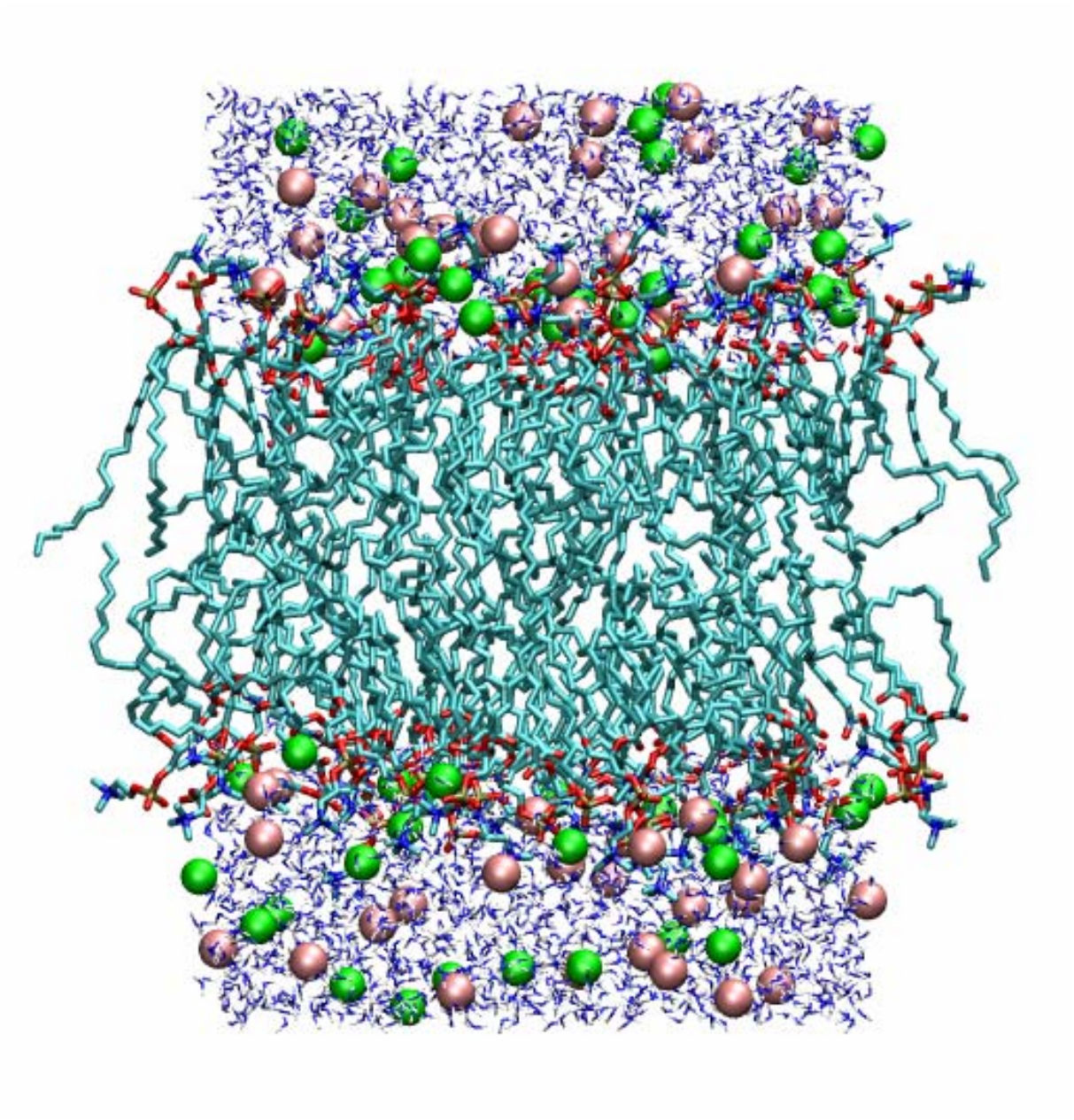

Figure 2:

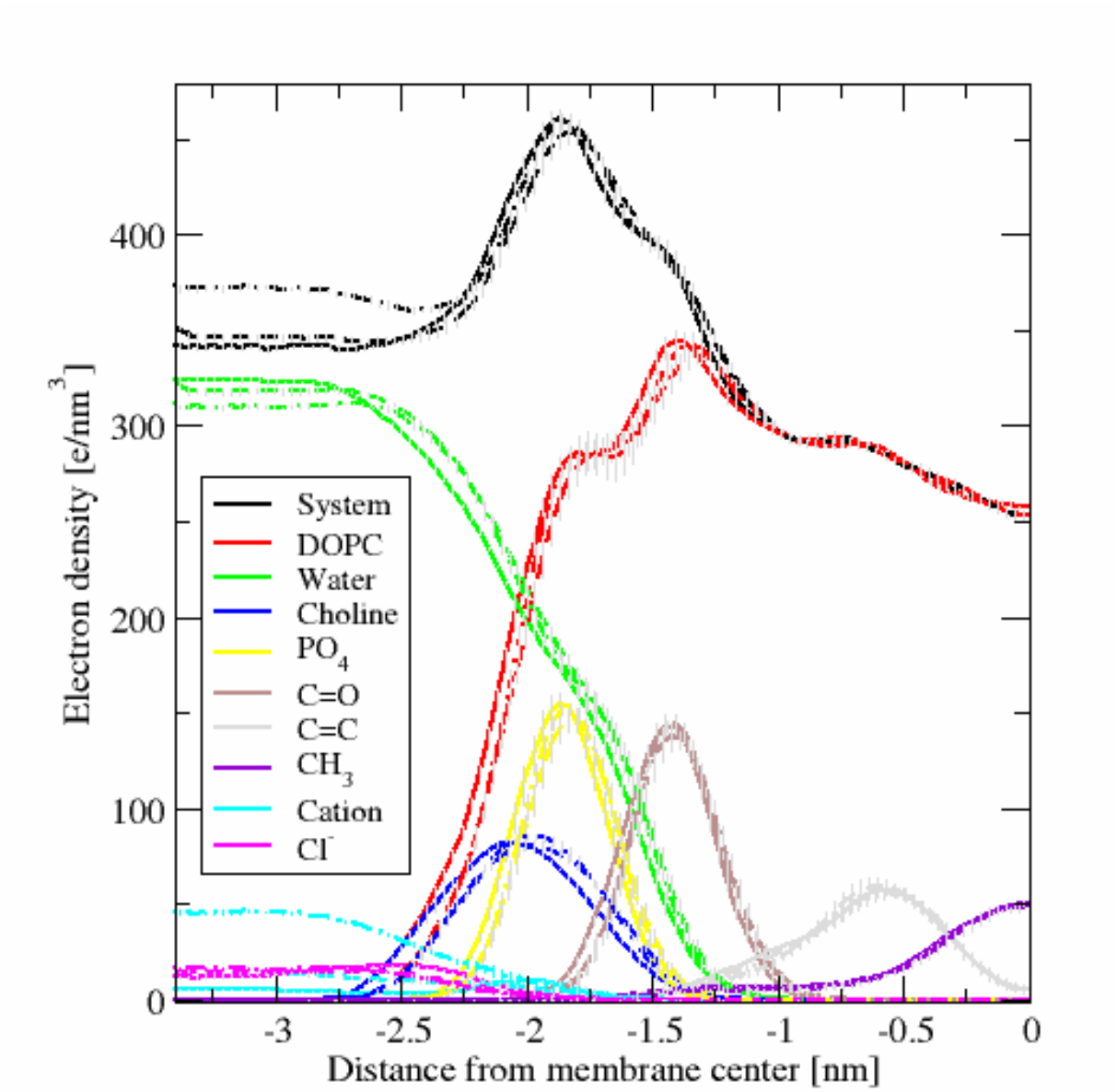
Electron density [e/nm^3]
Distance from membrane center [nm]
System
DOPC
Water
Choline
PO_4
C=O
C=C
CH_3
Cation
Cl^-
0
100
200
300
400
-3
-2.5
-2
-1.5
-1
-0.5
0

Figure 3:

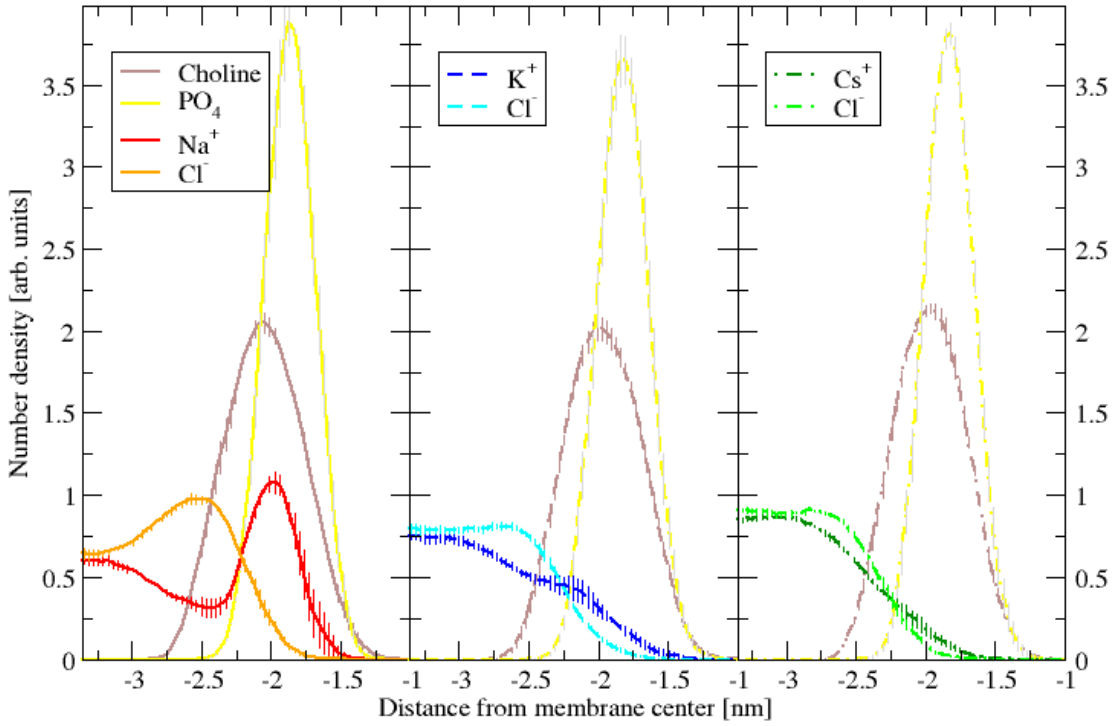
Choline
PO4
Na+
Cl-
K+
Cl-
Cs+
Cl-
Number density [arb. units]
Distance from membrane center [nm]
0
0.5
1
1.5
2
2.5
3
3.5
-3
-2.5
-2
-1.5
-1

Figure 4:

A)

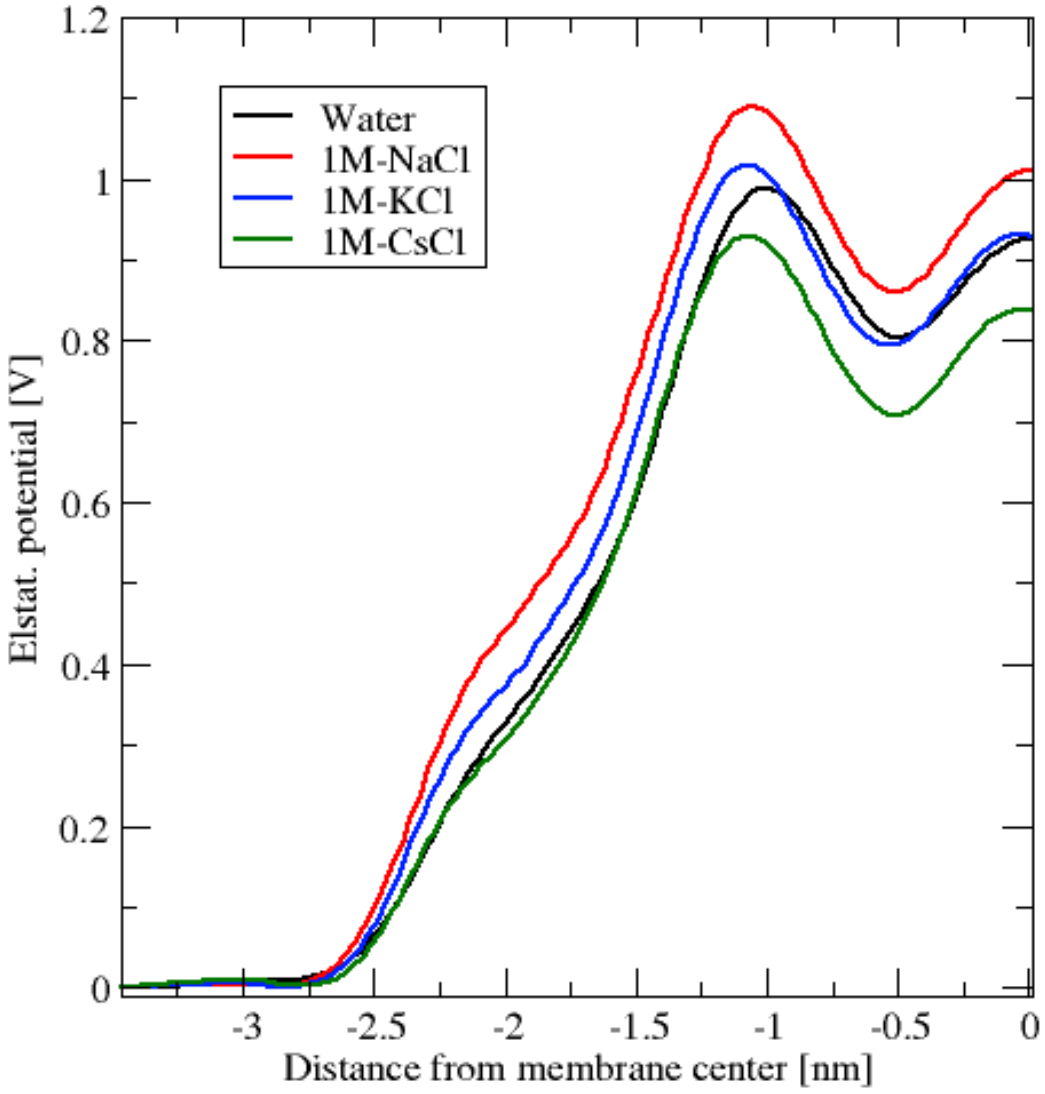
Water
1M-NaCl
1M-KCl
1M-CsCl
Elstat. potential [V]
Distance from membrane center [nm]
1.2
1
0.8
0.6
0.4
0.2
0
-3
-2.5
-2
-1.5
-1
-0.5
0

B)

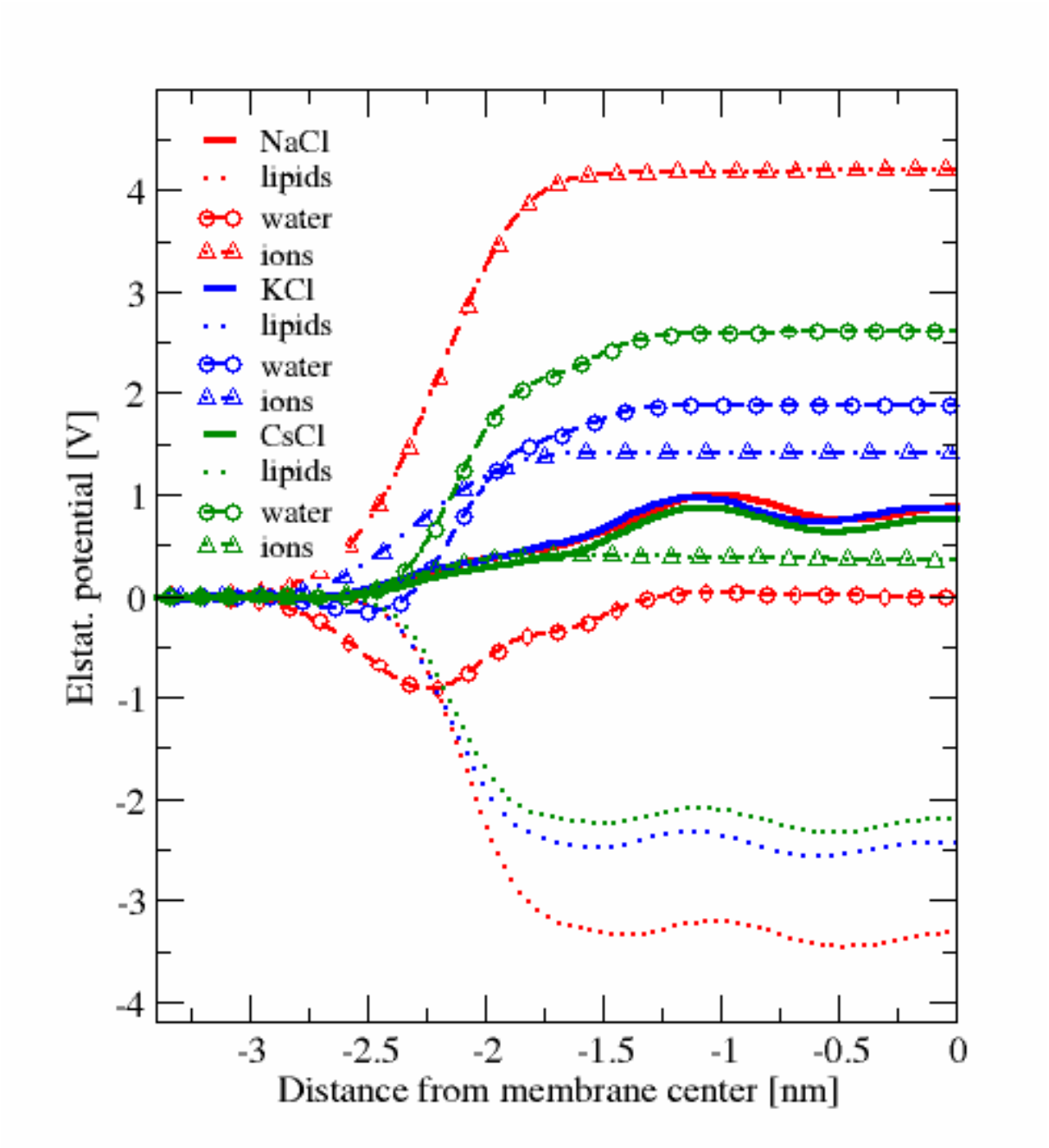
NaCl
lipids
water
ions
KCl
lipids
water
ions
CsCl
lipids
water
ions
Elstat. potential [V]
Distance from membrane center [nm]
4
3
2
1
0
-1
-2
-3
-4
-3
-2.5
-2
-1.5
-1
-0.5
0

Figure 5:

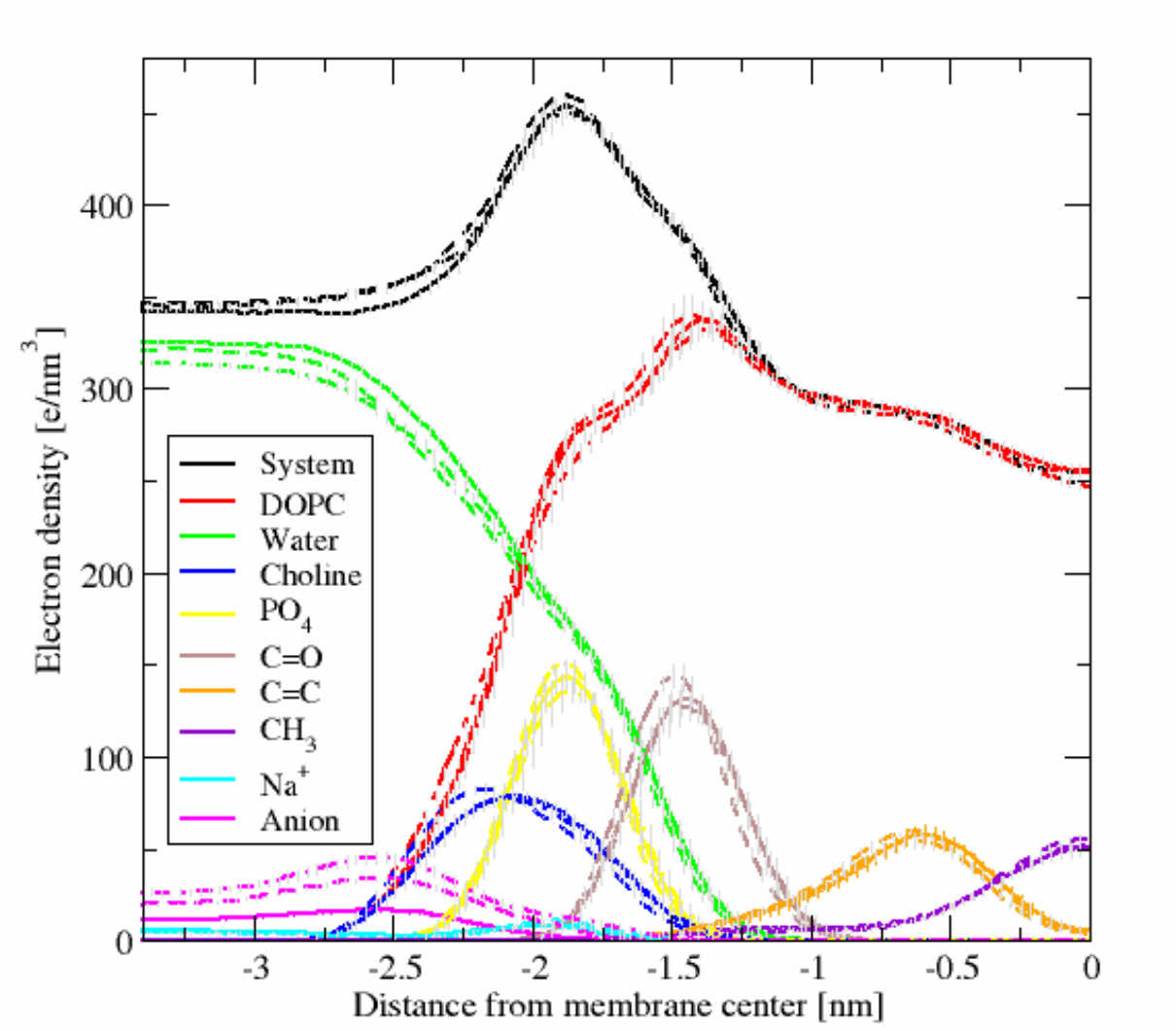
Electron density [e/nm^3]
Distance from membrane center [nm]
System
DOPC
Water
Choline
PO_4
C=O
C=C
CH_3
Na^+
Anion
0
100
200
300
400
-3
-2.5
-2
-1.5
-1
-0.5
0

Figure 6:

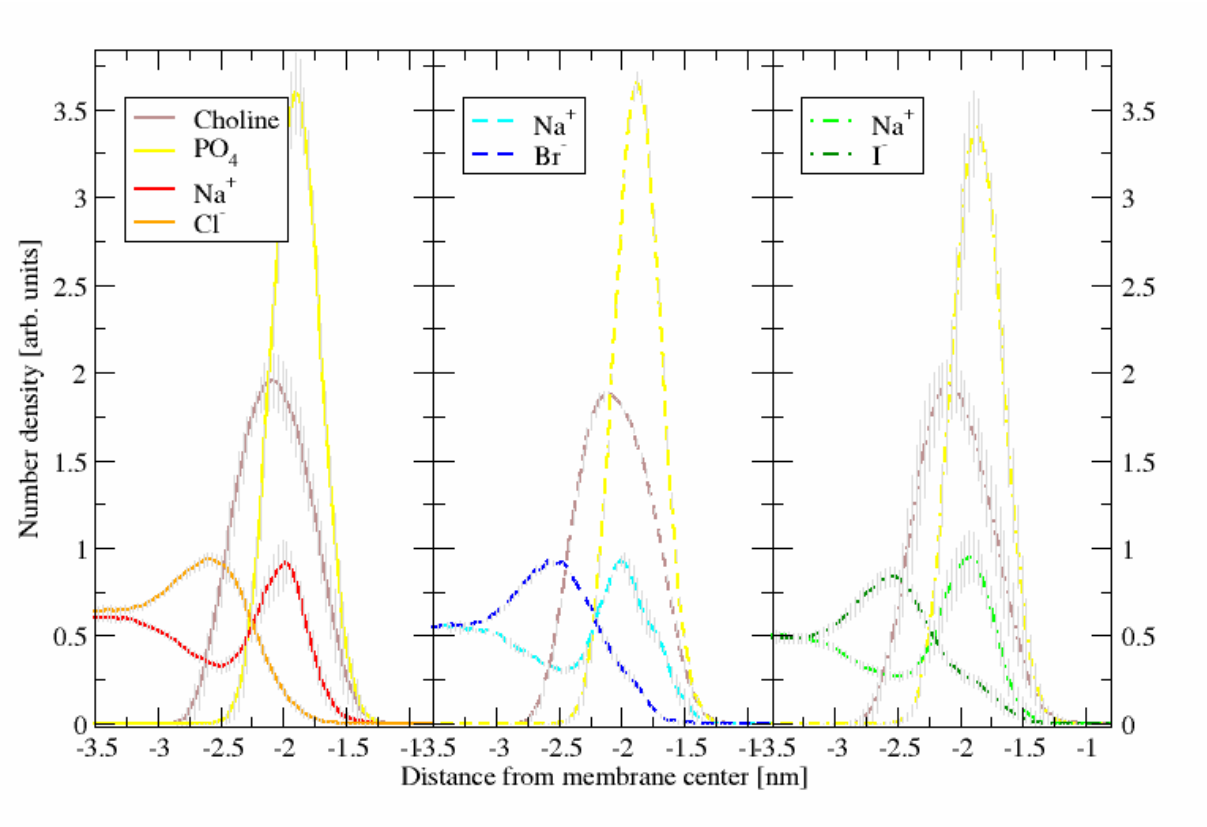
Choline
PO4
Na+
Cl-
Na+
Br-
Na+
I-
Number density [arb. units]
Distance from membrane center [nm]
0
0.5
1
1.5
2
2.5
3
3.5
-3.5
-3
-2.5
-2
-1.5
-1

Figure 7:

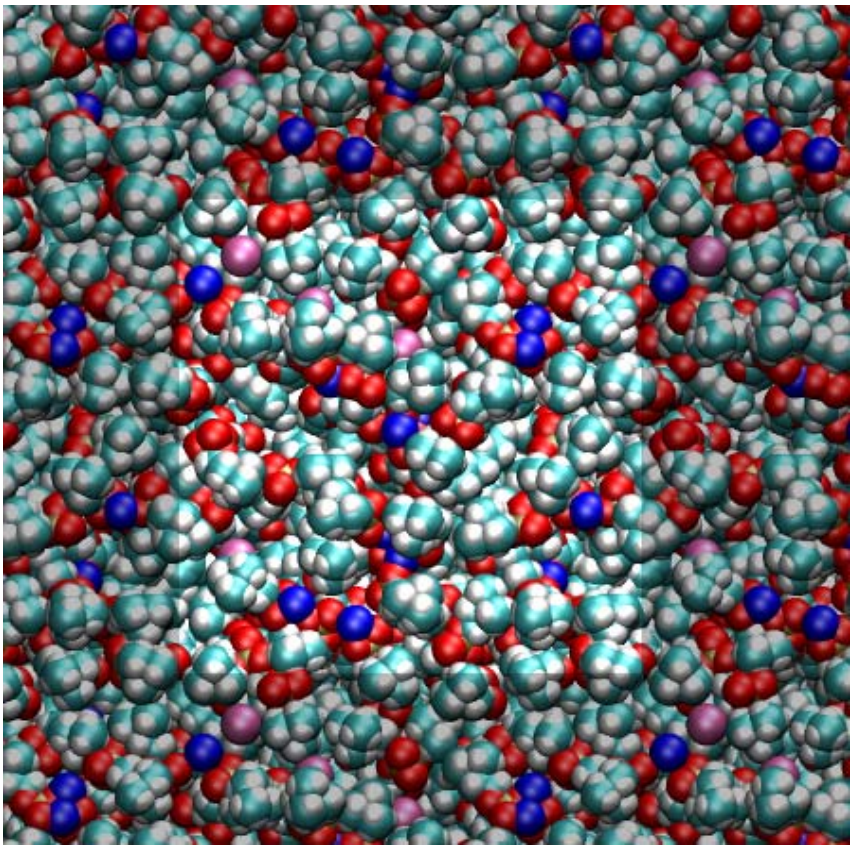

Figure 8:

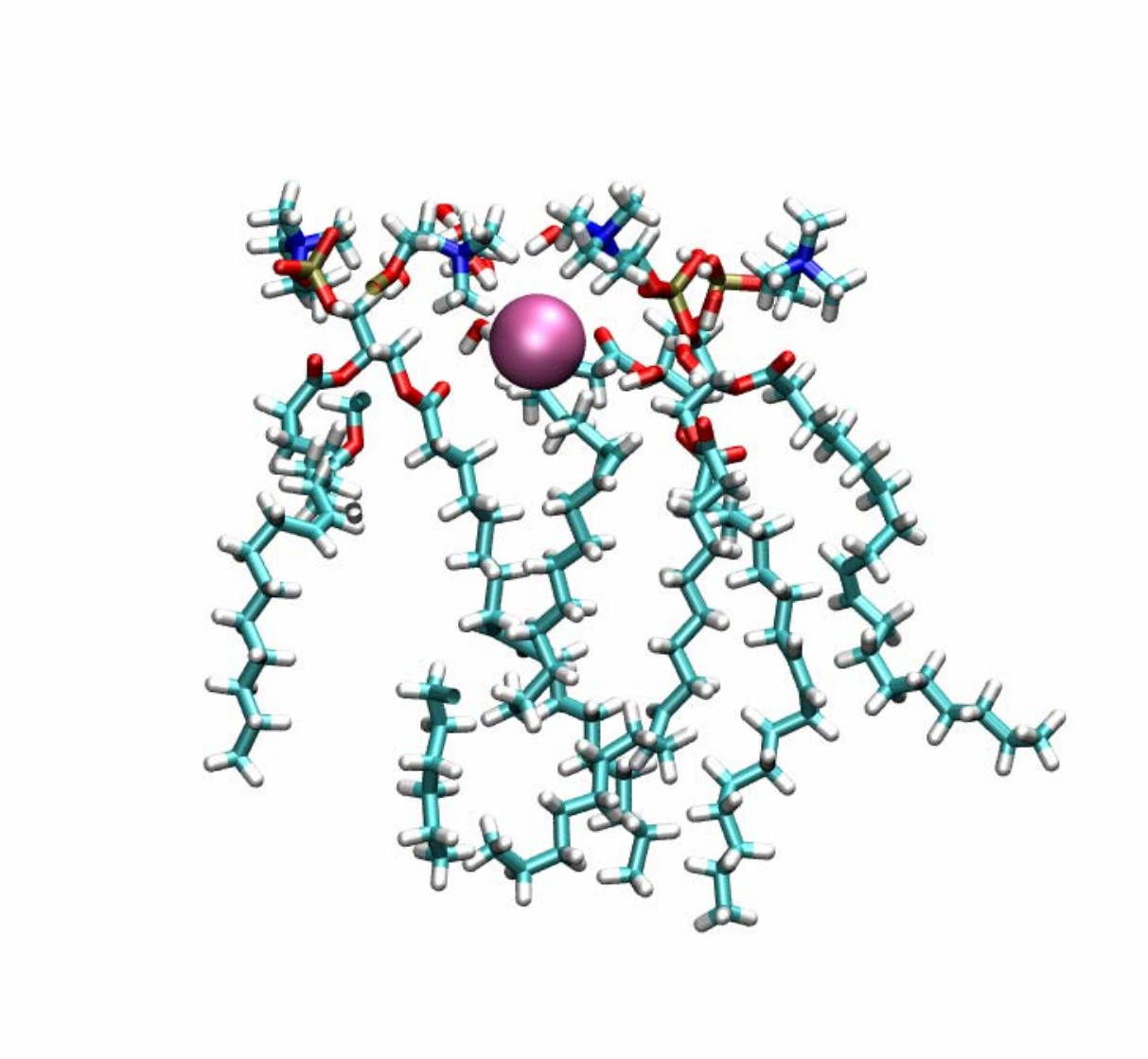

Figure 9:

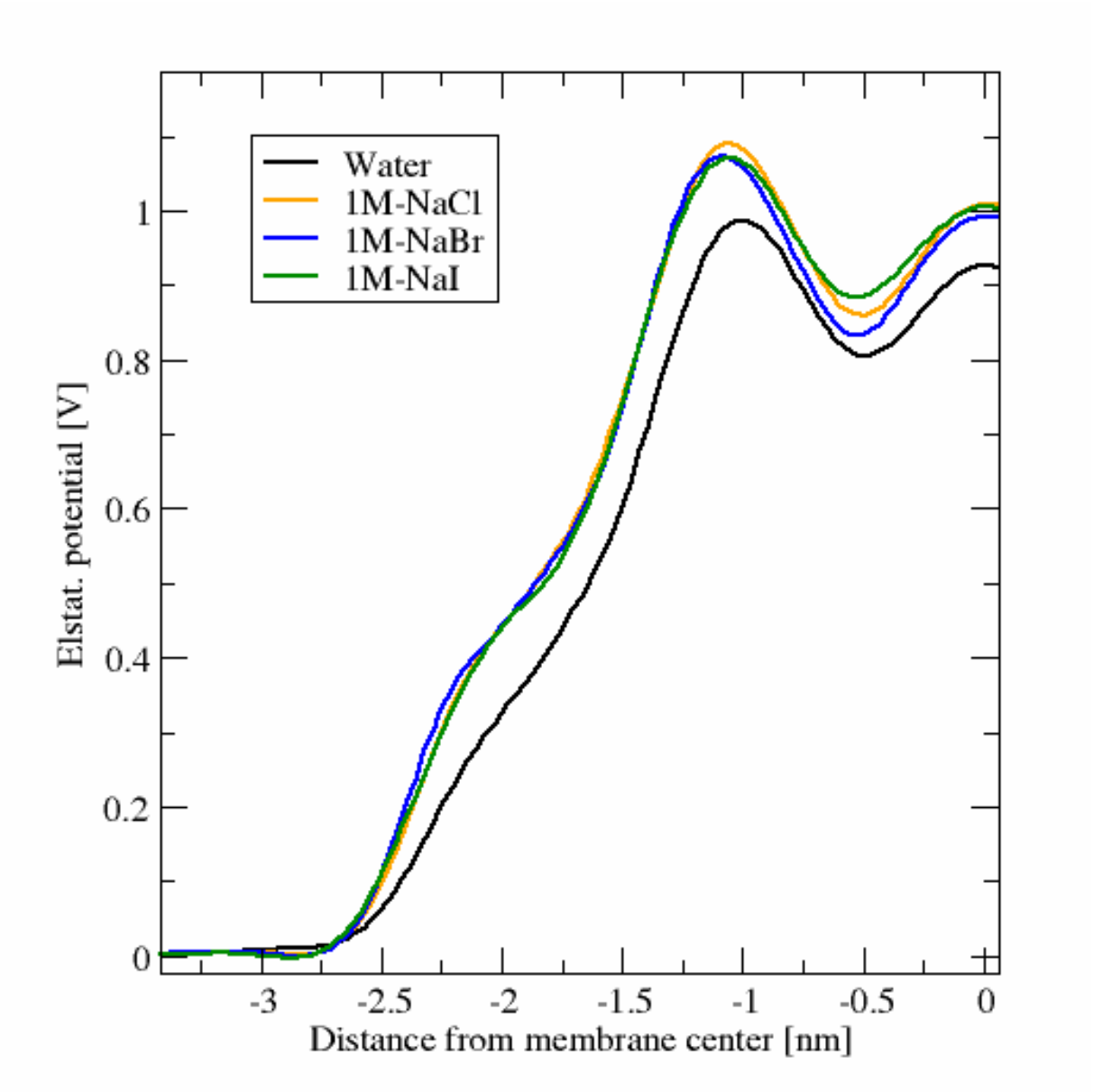
Water
1M-NaCl
1M-NaBr
1M-NaI
Elstat. potential [V]
0
0.2
0.4
0.6
0.8
1
-3
-2.5
-2
-1.5
-1
-0.5
0
Distance from membrane center [nm]

References:

(1) McLaughlin, S. *Annual Review of Biophysics and Biophysical Chemistry* **1989**, *18*, 113-136.

(2) Hodgkin, A. L.; Horowicz, P. *Journal of Physiology-London* **1960**, *153*, 404-412.

(3) Clarke, R. J.; Lupfert, C. *Biophysical Journal* **1999**, *76*, 2614-2624.

(4) Kunz, W.; Henle, J.; Ninham, B. W. *Current Opinion in Colloid & Interface Science* **2004**, *9*, 19-37.

(5) Petrache, H. I.; Zemb, T.; Belloni, L.; Parsegian, V. A. *Proceedings of the National Academy of Sciences of the United States of America* **2006**, *103*, 7982-7987.

(6) Aroti, A.; Leontidis, E.; Dubois, M.; Zemb, T. *Biophysical Journal* **2007**, *93*, 1580-1590.

(7) Leontidis, E.; Aroti, A.; Belloni, L.; Dubois, M.; Zemb, T. *Biophysical Journal* **2007**, *93*, 1591-1607.

(8) Garcia-Manyes, S.; Oncins, G.; Sanz, F. *Biophysical Journal* **2005**, *89*, 4261-4274.

(9) Garcia-Celma, J. J.; Hatahet, L.; Kunz, W.; Fendler, K. *Langmuir* **2007**, *23*, 10074-10080.

(10) Pabst, G.; Hodzic, A.; Strancar, J.; Danner, S.; Rappolt, M.; Laggner, P. *Biophysical Journal* **2007**, *93*, 2688-2696.

(11) Bockmann, R. A.; Hac, A.; Heimburg, T.; Grubmuller, H. *Biophysical Journal* **2003**, *85*, 1647-1655.

(12) Pandit, S. A.; Bostick, D.; Berkowitz, M. L. *Biophysical Journal* **2003**, *84*, 3743-3750.

(13) Gurtovenko, A. A.; Vattulainen, I. *Journal of Physical Chemistry B* **2008**, *112*, 1953-1962.

(14) Lee, S. J.; Song, Y.; Baker, N. A. *Biophysical Journal* **2008**, *94*, 3565-3576.

(15) Cordomi, A.; Edholm, O.; Perez, J. J. *J. Phys. Chem. B* **2008**.

(16) Bockmann, R. A.; Grubmuller, H. *Angewandte Chemie-International Edition* **2004**, *43*, 1021-1024.

(17) Cordomi, A.; Edholm, O.; Perez, J. J. *Journal of Physical Chemistry B* **2008**, *112*, 1397-1408.

(18) Van Der Spoel, D.; Lindahl, E.; Hess, B.; Groenhof, G.; Mark, A. E.; Berendsen, H. J. *J Comput Chem* **2005**, *26*, 1701-1718.

(19) Siu, S.; Vacha, R.; Jungwirth, P.; Bockmann, R. *The Journal of Chemical Physics* **2008**, *128*.

(20) Darden, T.; York, D.; Pedersen, L. *The Journal of Chemical Physics* **1993**, *98*, 10089-10092.

(21) Berendsen, H. J. C.; Grigera, J. R.; Straatsma, T. P. *J. Phys. Chem. A* **1987**, *91*, 6269 - 6271.

(22) Markovich, G.; Perera, L.; Berkowitz, M. L.; Cheshnovsky, O. *Journal of Chemical Physics* **1996**, *105*, 2675-2685.

(23) Smith, D. E.; Dang, L. X. *Chemical Physics Letters* **1994**, *230*, 209-214.

(24) Dang, L. X.; Schenter, G. K.; Glezakou, V. A.; Fulton, J. L. *Journal of Physical Chemistry B* **2006**, *110*, 23644-23654.

(25) Dang, L. X. *Journal of Physical Chemistry B* **1999**, *103*, 8195-8200.

(26) Auffinger, P.; Cheatham, T. E.; Vaiana, A. C. *J. Chem. Theory Comput.* **2007**, *3*, 1851-1859.

(27) Chen, A. A.; Pappu, R. V. *J. Phys. Chem. B* **2007**.

(28) Epand, R. F.; Epand, R. M.; Sterk, G. J.; Thijsse, P. A.; Sang, H.; Kraayenhof, R. *Biophysical Journal* **1996**, *70*, TUAM8-TUAM8.

(29) Benes, M.; Billy, D.; Benda, A.; Speijer, H.; Hof, M.; Hermens, W. T. *Langmuir* **2004**, *20*, 10129-10137.

(30) Jurkiewicz, P.; Sykora, J.; Olzynska, A.; Humplickova, J.; Hof, M. *Journal of Fluorescence* **2005**, *15*, 883-894.

(31) Horng, M. L.; Gardecki, J. A.; Papazyan, A.; Maroncelli, M. *Journal of Physical Chemistry* **1995**, *99*, 17311-17337.

(32) Benda, A.; Benes, M.; Marecek, V.; Lhotsky, A.; Hermens, W. T.; Hof, M. *Langmuir* **2003**, *19*, 4120-4126.

(33) Dertinger, T.; Pacheco, V.; von der Hocht, I.; Hartmann, R.; Gregor, I.; Enderlein, J. *Chemphyschem* **2007**, *8*, 433-443.

(34) Humpolickova, J.; Gielen, E.; Benda, A.; Fagulova, V.; Vercammen, J.; Vandeven, M.; Hof, M.; Ameloot, M.; Engelborghs, Y. *Biophysical Journal* **2006**, *91*, L23-L25.

(35) Wawrezinieck, L.; Rigneault, H.; Marguet, D.; Lenne, P. F. *Biophysical Journal* **2005**, *89*, 4029-4042.

(36) Sachs, J.; Crozier, P.; Woolf, T. *The Journal of chemical physics* **2004**, *121*, 10847-51.

(37) Liu, Y.; Nagle, J. *Physical Review E* **2004**, *69*, 040901.

(38) Jurkiewicz, P.; Olzynska, A.; Langner, M.; Hof, M. *Langmuir* **2006**, *22*, 8741-8749.

(39) Sykora, J.; Jurkiewicz, P.; Epand, R. M.; Kraayenhof, R.; Langner, M.; Hof, M. *Chemistry and Physics of Lipids* **2005**, *135*, 213-221.

(40) *Biophysical Journal* **2008**, *94*, 3565.

(41) Pandit, S.; Bostick, D.; Berkowitz, M. *Biophys. J.* **2003**, *84*, 3743-3750.

(42) Sachs, J. N.; Woolf, T. B. *Journal of the American Chemical Society* **2003**, *125*, 8742-8743.

(43) Sachs, J. N.; Nanda, H.; Petrache, H. I.; Woolf, T. B. *Biophysical Journal* **2004**, *86*, 3772-3782.

(44) Perera, L.; Berkowitz, M. *The Journal of Chemical Physics* **1991**, *95*, 1954-1963.

(45) Vrbka, L.; Mucha, M.; Minofar, B.; Jungwirth, P.; Brown, E. C.; Tobias, D. J. *Current Opinion in Colloid & Interface Science* **2004**, *9*, 67-73.